

Estimation of multiple density-depth parameters from gravity inversion: Application to detached hanging wall systems of strike limited listric fault morphologies

V. Chakravarthi* and M. Pramod Kumar

Received: September 30, 2013; accepted: May 20, 2014 published on line: December 12, 2014

Resumen

Se desarrolló un algoritmo de inversión para estimar simultáneamente la geometría de plano de falla y los parámetros que pertenecen a cualquiera de las densidades o profundidades de múltiples formaciones geológicas, con el sistema de colgado en la pared, en un plano de fractura limitada de las anomalías de gravedad observadas. Se describen planos de falla de las estructuras mediante funciones polinómicas de grado arbitrario pero específico. La aplicabilidad del algoritmo se demostró tanto en las anomalías artificiales y reales de la gravedad de campo. En el ejemplo de síntesis se añadió ruido pseudoaleatorio a las anomalías de gravedad de la estructura antes de la inversión. En la inversión de anomalías de gravedad, producidos por una estructura sintética, se encontró que los parámetros estimados más o menos imitan los parámetros obtenidos, incluso en presencia de ruido aleatorio. Las densidades y profundidades estimadas de las formaciones de inversión independiente de anomalías de gravedad del mundo real desde el margen de la subcuenca Chintalpudi en la India se correlacionan bien con la información disponible de la perforación.

Palabras clave: morfología de fallas lístricas, falla finita, variaciones arbitrarias de densidad-densidad, anomalía de gravedad, inversión.

Abstract

An inversion algorithm is developed to simultaneously estimate the fault plane geometry and the parameters pertaining to either densities or depths of multiple geologic formations within the hanging wall system of a strike-limited listric fault from the observed gravity anomalies. Fault planes of the structures are described by polynomial functions of arbitrary but specific degree. The applicability of the algorithm is demonstrated on both synthetic and real field gravity anomalies. In the synthetic example, pseudorandom noise is added to the gravity anomalies of the structure prior to inversion. From the inversion of gravity anomalies produced by a synthetic structure it was found that the estimated parameters more or less mimic the true parameters even in the presence of random noise. The estimated densities and depths of the formations from independent inversion of real-world gravity anomalies from the margin of the Chintalpudi sub-basin in India correlate well with the available drilling information.

Key words: listric fault morphology, finite strike, arbitrary density-density variations, gravity anomaly, inversion.

V. Chakravarthi*
 M. Pramod Kumar
 Centre for Earth & Space Sciences
 University of Hyderabad
 Gachibowli, Hyderabad – 500 046 (A.P.)
 India
 *Corresponding author:vcvarthi@rediffmail.com

Introduction

Listric faults are curved normal faults in which the fault surface is concave upwards because the main detachment fracture follows a curved path rather than a planar path. Because of the non-planar nature of listric fault planes it is often difficult to estimate the amount of extension from surface geological observations of dip and throw of the faults (McKenzie, 1978). On the other hand, the displaced rock masses on either side of such fault planes can create lateral contrasts in subsurface densities and accordingly generate detectable step-like gravity anomalies across the fault planes. These anomalies can be appropriately analyzed to quantify the fault morphology.

Although fault morphologies more often than not possess non-planar fault planes (Brady *et al.* 2000; Goussav *et al.* 2006; McKenzie and Jackson 2012), many existing algorithms assume planar surfaces for the fault planes to analyze the gravity anomalies. For example, Thanassoulas *et al.* (1987) developed a method and a computer program in Basic, Murthy and Krishnamacharyulu (1990) devised an algorithm and a relevant code in Fortran to estimate the parameters of fault structures from the observed gravity anomalies. Abdelrahman *et al.* (1989) proposed a method to determine the dip angle of a fault plane from the maximum positive and negative amplitudes of gravity anomalies, where the relative movement between two semi-infinite horizontal slabs was confined to a planar surface. Rao *et al.* (2003) used generalized inversion and single value decomposition techniques to analyze the gravity anomalies of fault structures. Abdelrahman *et al.* (2003) presented two approaches to determine the depth and amplitude coefficient, related to the density contrast and the thickness of a buried faulted slab using numerical horizontal derivative anomalies obtained from 2D gravity data. On the other hand, Stavrev and Reid (2010) used the concept of extended Euler homogeneity of potential fields to analyze the gravity anomalies of a thick faulted slab. Recently, Essa (2013) developed an algorithm that make use of numerical first horizontal derivatives computed from the observed gravity anomaly to estimate the depth and the dip angle of a buried fault structure, whereas Toushmalani (2013) proposed a technique using particle swarm optimization to interpret the anomalies.

The above 2D strategies find limited application when analyzing the gravity anomalies of listric fault morphologies because

i) the fault planes associated with these structures are often non-planar in nature, and ii) the density of the sedimentary load within the hanging wall is rarely uniform (Maxant 1980; Moral *et al.* 2000; Rybakov *et al.* 2000; Nagihara and Hall, 2001; Adriasyah and McMechan, 2002; Gómez-Ortiz 2005). Realizing the fact that the density of sedimentary rocks varies with depth, Rao (1985) used a quadratic density function, Sundararajan and Brahman (1998) adopted a linear density function, and Chakravarthi and Sundararajan (2004) used a parabolic density function to analyze the gravity anomalies of fault structures, again treating the fault structures as 2D with fault planes as planar surfaces.

Martín-Atienza and García-Abdeslem (1999) developed a technique using a quadratic density function to compute the gravity anomalies of geologic sources bounded either laterally or vertically by continuous functions. Though this method can be used to simulate the geometries of listric fault sources to compute gravity anomalies, it is efficient only for 2D sources. Based on the fact that the fault structures on the continental regions often possess finite strike lengths (Peirce and Lipkov 1988), Chakravarthi (2011) developed an automatic inversion to interpret the gravity anomalies of 2.5D strike listric fault sources, where the fault planes are described by polynomial functions of arbitrary degree and the variation of density within the hanging wall by a parabolic density function. This technique is effective when the density contrast of sedimentary load within the hanging wall decreases monotonically with depth. On the other hand, Chakravarthi (2010) devised a strategy with a relevant code in Fortran to compute the gravity anomalies of strike limited listric fault morphologies, where the hanging wall was assumed to consist in several geologic formations of differing densities and thicknesses. To realize forward modeling, this method requires the coefficients of the polynomial (used to describe the fault plane geometry) and the parameters pertaining to both thickness and densities of formations within the hanging wall as part of input, which in reality are not known a priori. Therefore, a need exists to develop an appropriate algorithm to estimate these parameters from the observed gravity anomalies (inverse process).

In the present paper, we develop a gravity inversion technique using ridge regression to estimate the parameters of a listric fault structure from the observed gravity anomalies, where the structure is assumed as a 2.5D source with the detached hanging wall consists in several geologic formations; each one

possesses its own density and thickness. The forward modeling algorithm of Chakravarthi (2010) is used to compute the gravity response of a listric fault structure whereas the business logic of the present inversion estimates the unknown parameters based on the differences between the measured and model gravity anomalies. In this case, the unknown parameters to be estimated from a gravity profile are: depths or densities of formations (because the density and the volume of the source cannot be determined without prior information about one of them) and coefficients of a polynomial used to describe the fault plane as a function of depth. The validity and applicability of the technique are demonstrated with both synthetic and real field gravity anomalies. The estimated parameters are compared with the assumed parameters in case of synthetic example and with measured density-depth data in case of a real field example.

Gravity anomalies of strike limited listric fault sources

In a Cartesian co-ordinate system, let the z -axis be positive vertically downwards and the x -axis transverse to the strike of a listric fault source whose geometry is shown in Figure 1. The structure is located between the limits, z_T and z_B , along the z -axis and along the x -axis, the structure is bounded by a function, $\zeta(z)$, on the left and towards the right it is extending to infinity. Further, the structure is having a limited strike length of $2Y$ along the y -axis perpendicular to the xz plane. The detached hanging wall of the structure consists of several geological formations, N in number.

Further, each formation has its own density, ρ_i , $i = 1, 2, \dots, N$. For such a structure, the gravity anomaly, $g_{\text{mod}}(x_j, z_j)$, at any point, $P(x_j, z_j)$, on the profile, CD , that runs along the x -axis and bisects the strike length, $2Y$, of the structure outside the source region is given by (Chakravarthi 2010),

$$g_{\text{mod}}(x_j, z_j) = 2G \sum_{k=1}^N \Delta\rho_k \int_{z_k}^{z_{k+1}} \left[\frac{\tan^{-1} \frac{Y}{(z - z_j)}}{-(z - z_j) \sqrt{(\zeta(z) - x_j)^2 + (z - z_j)^2 + Y^2}} \right] dz, \quad (1)$$

where, G is the universal gravitational constant, $\Delta\rho_k$ is the density contrast of the k^{th} formation, z_k and z_{k+1} represent the depths to the top and bottom bounding surfaces of the respective formation within the hanging wall. Further, the fault plane is described by a function, $\zeta(z) = \sum_{l=0}^{N1} f_l z^l$, where f_l represent the coefficients of the polynomial. It is convenient to solve equation (1) by means of a numerical method rather than an analytical method because the polynomial, $\zeta(z)$, may take any degree (Chakravarthi 2010). In case the profile runs at an offset, s , (such as the profile, $C'D'$ in Figure 1) across the strike then the anomalous field at any point on the profile outside the source region can be calculated as in equation (1) but by substituting, $Y - s$ and $Y + s$ for Y (Chakravarthi, 2010). Also if the profile runs at an angle, α , with the x -axis then x_j in Eq. (1) needs to be replaced by $x_j \cos\alpha$ (Chakravarthi and Ramamma, 2013).

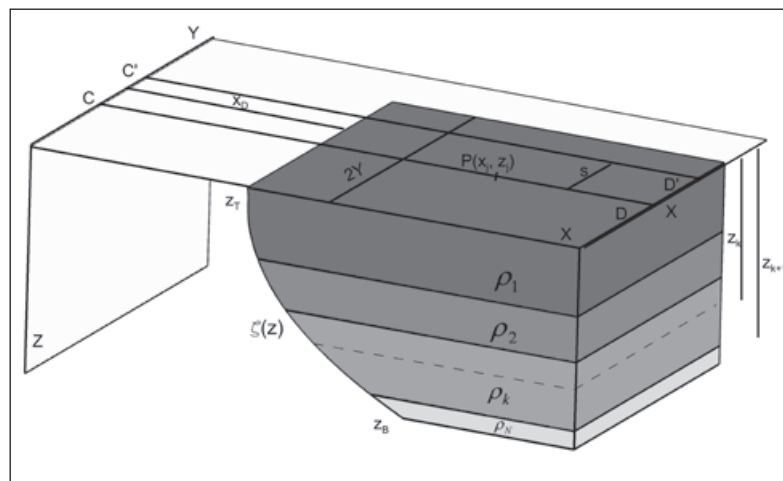


Figure 1. Schematic representation of a strike limited listric fault source. The detached downthrown block (hanging wall) is consisting of N horizontal formations with differing depths and densities. The limited strike length prevents the structure to represent as a 2D source.

Inversion of gravity anomalies

Inversion of gravity anomalies of listric fault sources is tantamount to a mathematical exercise of trying to fit the observed gravity anomalies to the anomaly expression and solve the unknown parameters within specified convergence criteria such that the inferred model is geologically acceptable. We propose two variants of inversion to analyze the gravity anomalies: i) densities and coefficients of the polynomial, $\zeta(z)$, are estimated while keeping the depths of the density interfaces intact, and ii) depths and coefficients of the polynomial are estimated while keeping the densities of the formations intact.

In either case, the interpretation starts by assigning approximate parameters of the structure (densities or depths of the formations) supplemented by drilling/other geophysical methods. To start with, the algorithm identifies the approximate location of the fault plane, $x_{D'}$ (Figure 1) on the profile at a point at which the corresponding anomalous field reaches to one half the maximum anomaly (Chakravarthi 2011). Initially, this value is assigned to the constant term, f_0 , of the polynomial, $\zeta(z)$, while the other coefficients are set to zero. These initial parameters of the structure are used to calculate the modeled gravity anomalies, $g_{\text{mod}}(x_j, z_j)$, using equation (1). Because the initial parameters are only approximate, the modeled gravity anomalies deviate from the observed anomalies. The difference between the observed anomalies, $g_{\text{obs}}(x_j, z_j)$, and the modeled anomalies, $g_{\text{mod}}(x_j, z_j)$, at any point, $P(x_j, z_j)$, on the profile can be expressed as a cumulative effect of a truncated Taylor's series expansion involving the partial derivatives of anomaly with respect to each unknown parameter and corresponding increment as

$$g_{\text{obs}}(x_j, z_j) - g_{\text{mod}}(x_j, z_j) = \sum_{k=1}^N \frac{\partial g_{\text{mod}}(x_j, z_j)}{\partial a_k} da_k + \sum_{m=0}^{N-1} \frac{\partial g_{\text{mod}}(x_j, z_j)}{\partial f_m} df_m, \quad (2)$$

where, da_k are increments/decrements in the parameters pertaining to either densities or depths and df_m are the increments/decrements to the coefficients of the polynomial used to describe the fault plane.

Linear equations similar to equation (2) are constructed for each observation on the profile and $(N + N1 + 1)$ normal equations are formed and solved by minimizing the misfit, J , between the observed and modeled gravity anomalies defined by

$$\sum_{j=1}^{N_{\text{obs}}} [g_{\text{obs}}(x_j, z_j) - g_{\text{mod}}(x_j, z_j)]^2 \quad (3)$$

using ridge regression (Marquardt, 1970). Here, N_{obs} stands for the number of observations on the profile. The relevant system of normal equations can be expressed in a matrix form as

$$(A + \delta I) X = B, \quad (4)$$

where, A is $n \times n$ matrix whose elements $A_{nj'}$ are given by

$$A_{nj'} = \sum_{n=1}^{N+N1+1} \sum_{m=1}^{N_{\text{obs}}} \frac{\partial g_{\text{mod}}(x_m, z_m)}{\partial a_{j'}} \frac{\partial g_{\text{mod}}(x_m, z_m)}{\partial a_n}, \quad (5)$$

$$X = da_n, \quad (6)$$

$$B = \sum_{m=1}^{N_{\text{obs}}} [g_{\text{obs}}(x_m, z_m) - g_{\text{mod}}(x_m, z_m)] \frac{\partial g_{\text{mod}}(x_m, z_m)}{\partial a_{j'}}, \quad j' = 1, 2, \dots, N + N1 + 1 \quad (7)$$

where, a_n , $n = 1, 2, \dots, N + N1 + 1$ are the number of unknown parameters and da_n represents the corresponding improvements in the parameters. δ is the damping factor and I is a diagonal matrix containing the diagonal elements of the matrix A . The application of ridge regression is described by Chakravarthi and Sundararajan (2006). The partial derivatives required in Eq. (5) and Eq. (7) are evaluated numerically (Chakravarthi *et al.* 2001), which involves the calculation of the rate of change of the gravity anomaly with respect to each unknown parameter. The improvements, da_n , solved from Eq. (4) are used to update the existing parameters and the exercise repeats until i) the specified number of iterations completed or ii) the misfit becomes less than the predefined allowable error or iii) the damping factor, δ , assumes an unusually large value (Chakravarthi, 2003).

Examples

The applicability of the algorithm is demonstrated on both synthetic and real field gravity anomalies. In either case the measurement is made at $z_j = 0$ km.

Theoretical example

Figure 2a shows a set of noisy gravity anomalies produced by a synthetic listric fault model, whose geometry is shown in Figure 2b. The structure has a half strike length of 50 km (Figure 2b). The anomalies (shown as solid line in Figure 2a) are produced at zero offset

in the interval $x_j \in [0, 80 \text{ km}]$. In this case, the pseudorandom noise was Gaussian, with zero mean and a standard deviation of 0.14 mGal. The foot wall remains intact and undisturbed, whereas the detached hanging wall consists of four formations: massive basalt of 3.5 km thick at the top is followed successively by 1.5 km thick sediments, 3 km thick vesicular basalt and 2.0 km thick compacted sediments above the basement. The model densities of the formations are given in Table 1 and shown in Figure 2c. In the present case, a 6th degree polynomial with a set of seven arbitrarily chosen coefficients (Table 2) is used to describe the fault plane geometry (shown as solid line in blue in Figure 2b).

We have used two prong strategies to analyze the gravity anomalies as described in section 3. Initially, the densities of the formations and polynomial coefficients (to describe the fault plane geometry) are estimated from the noisy anomalies (shown in Figure 2a) while keeping the depths of density interfaces unchanged, and secondly the depths of the interfaces and coefficients of the polynomial are estimated keeping the densities intact. Further, in either

case a 2nd degree polynomial is used (instead of a 6th degree) to describe the fault plane in the inversion to study its effect on the interpretation, if any.

Inversion of noisy anomalies to estimate densities and fault plane geometry

The noisy anomalies (Figure 2a) were subjected to inversion assuming an initial density of 2.0 g/cm³ for each of the subsurface formation (Table 1 and Figure 2c). The algorithm calculates the density contrast of each formation and uses them to compute the gravity effect of the structure. The approximate location of the fault plane identified by the algorithm is at 30.07 km on the profile. Initially, this value has been assigned to the first coefficient of the polynomial, f_0 , whereas other coefficients are set to zero as described in the text. For such an inversion, the algorithm had performed 69 iterations before it got terminated as the misfit, J , fell below a predefined allowable error of 0.01 mGal. No significant improvements either in densities or coefficients of the polynomial are observed beyond the 69th iteration (Figure 3b).

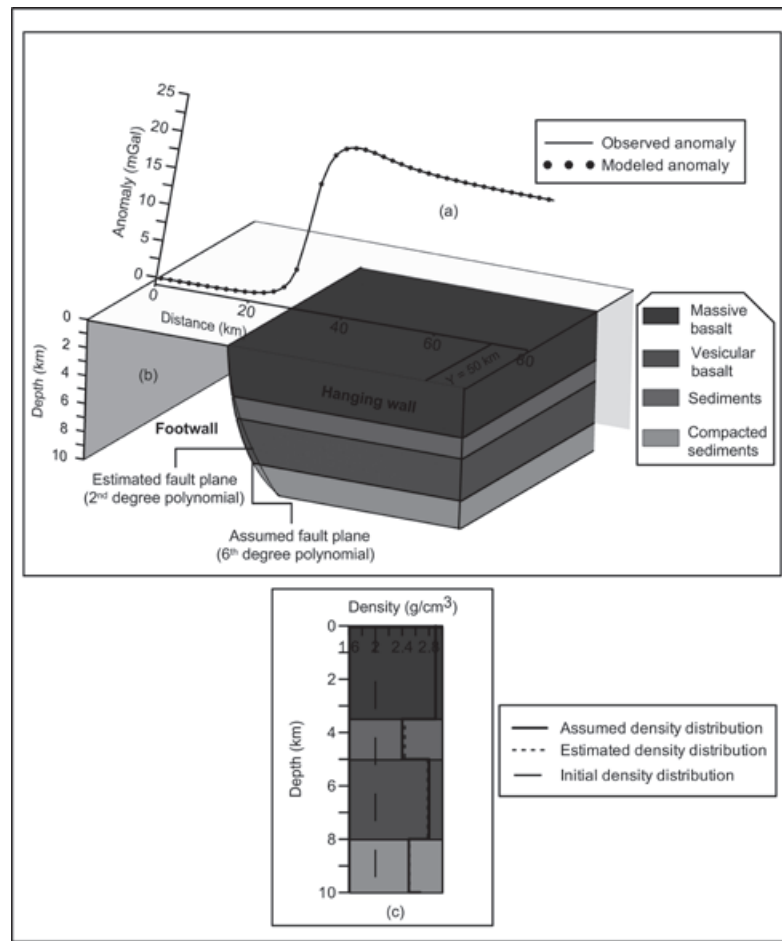
Table 1. Assumed and estimated densities in case of synthetic example

Formation	Assumed density (g/cm ³)	Initial density (g/cm ³)	Estimated density (g/cm ³)	Error (%)
Compact basalt	2.9	2.0	2.89	0.34
Sediments	2.4	2.0	2.44	1.67
Vesicular basalt	2.8	2.0	2.78	0.71
Compacted sediments	2.5	2.0	2.51	0.4

Table 2. Assumed and estimated coefficients of the polynomial, $\zeta(z)$, synthetic example

Coefficient	Assumed coefficients of the 6 th degree polynomial	Estimated coefficients of the 2 nd degree polynomial in case of density and fault plane inversion	Estimated coefficients of the 2 nd degree polynomial in case of depth and fault plane inversion
f_0	30.01900944	30.036317825	30.029928207
f_1	0.09650391535	0.070503563	0.076575279
f_2	0.1845273787	0.106036872	0.110244833
f_3	-0.07319248817		
f_4	0.01707929702		
f_5	-0.001753613786		
f_6	7.009779208E-005		

Figure 2. (a) Observed and modeled noisy gravity anomalies, (b) four layered hanging wall system of a synthetic listric fault source with assumed and modeled fault planes described by 6th and 2nd degree polynomials, (c) assumed, initial and modeled densities. Depths of density interfaces are fixed during inversion.



The modeled gravity anomalies (shown as a solid dots in Figure 2a) at the end of the 39th iteration closely fit the observed ones. A maximum error of 0.044 mGal between the observed and modeled gravity anomalies is observed exactly at the 36th km on the profile (Figure 3a). The value of J had reduced drastically from its initial value of 3550019 mGal² to 1.43 at the end of the 34th iteration and then to 0.001 at the end of the concluding iteration (Figure 3b). The estimated density parameters and coefficients of the 2nd degree polynomial from the inversion are given Table 1 and Table 2 and shown graphically in Figure 2c (dashed line) and 2b (solid line) respectively. The errors (%) between the assumed and estimated densities are given in Table 1. Further, the changes in each estimated parameter (densities and coefficients of the 2nd degree polynomial) against the iteration number are shown in Figure 3b.

It is to be noted from Figure 2b that the modeled fault plane by a 2nd degree polynomial marginally deviates from the assumed fault plane described by a 6th degree polynomial.

The estimated densities (Table 1 and Figure 2c) pertaining to two sedimentary pulses at different depths are marginally overestimated, whereas the densities of compact and vesicular basalts are slightly underestimated. Such an error between assumed and estimated densities is acceptable considering the presence of significant level of pseudorandom noise in the anomalies produced by the structure. Therefore, the fault plane whether it is described by a 2nd degree or a 6th degree does not appreciably affect the fault plane geometry and estimated densities of the structure.

Inversion of noisy anomalies to estimate depths and fault plane geometry

The inversion process is repeated to estimate the depths of the four concealed density interfaces and three coefficients of the polynomial by keeping the density parameters unchanged. In this case, the initial depths assigned to four density interfaces are given in Table 3 and shown in Figure 4c (dotted lines). The initial depths of the density interfaces are significantly different from the assumed/true

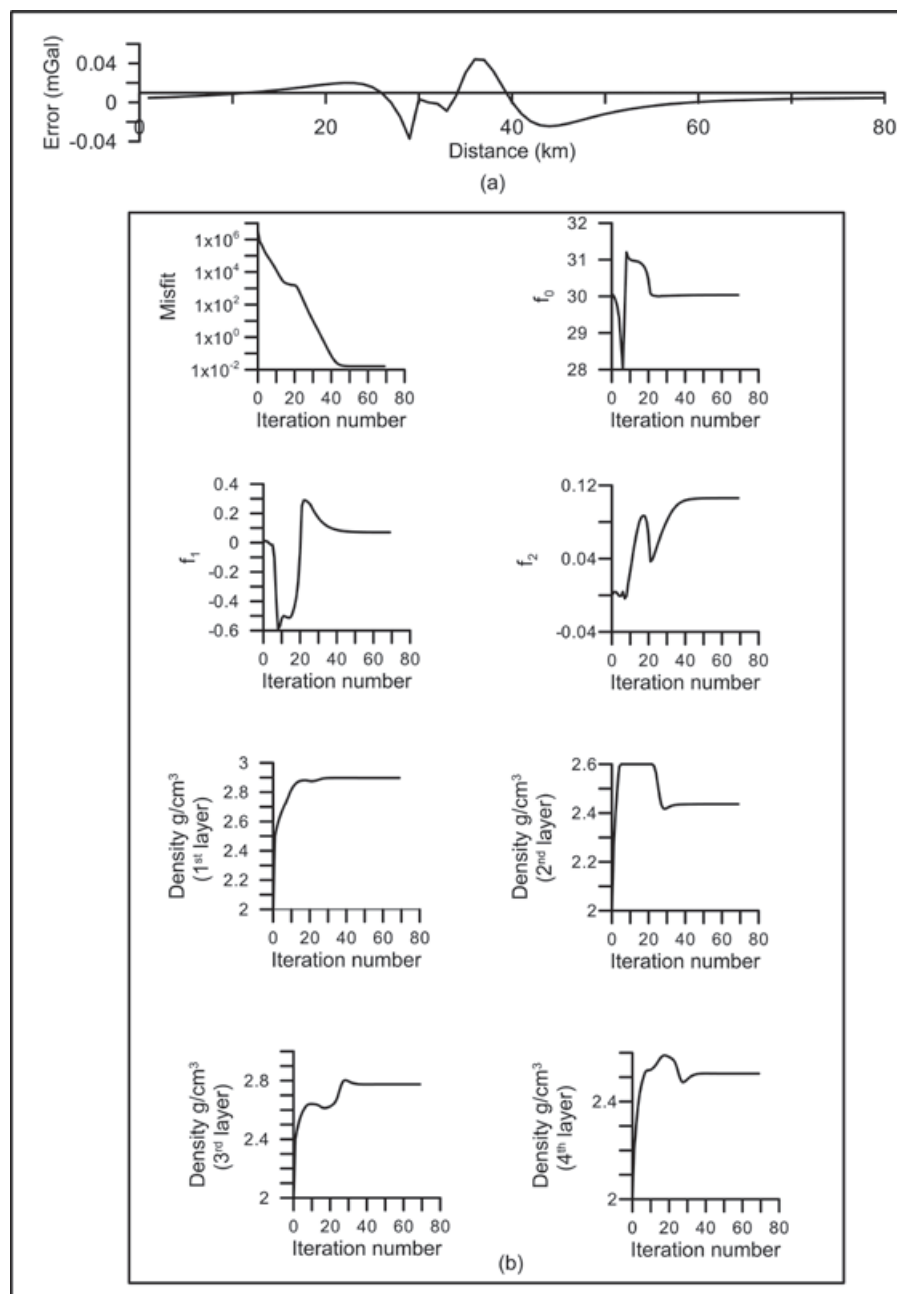


Figure 3. (a) Error analysis between the observed and modeled gravity anomalies, (b) Changes in misfit, coefficients of a 2nd degree polynomial, and densities of subsurface formations against the iteration number.

Table 3. Assumed and estimated depths to density interfaces, synthetic example.

Interface	Assumed depth (km)	Initial depth (km)	Estimated depth (km)	Error (%)
Compact basalt/sediments	3.5	1.5	3.44	1.71
Sediments/ Vesicular basalt	5.0	3	4.8	4.0
Vesicular basalt/compact sediments	8.0	5	7.6	5.0
Compact sediments/basement	10.0	8	9.57	4.3

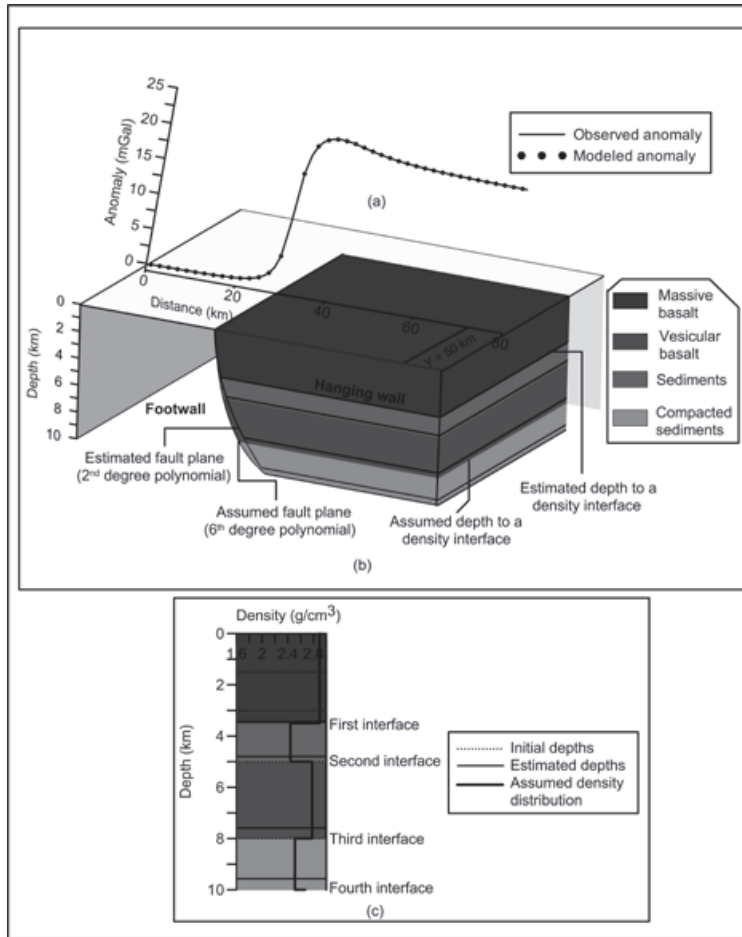


Figure 4. (a) Observed and modeled noisy gravity anomalies, (b) four layered hanging wall system of synthetic listric fault source with assumed and modeled fault planes described by 6th and 2nd degree polynomials, (c) assumed and estimated depths to density interfaces. Densities of the formations (shown as step line) are remain unchanged during inversion.

model parameters. As in the previous case, the approximate location of the fault plane identified by the algorithm at 30.07 km was assigned to the first coefficient of the polynomial, f_0 , whereas the other coefficients were set to zero. For such an inversion, the algorithm took 45 iterations before it got terminated. The misfit, J , had reduced from its initial value of 45565.3 mGal² for the starting model to 0.7 at the end of 19th iteration and then slowly to 0.004 mGal at the end of the 45th iteration (Figure 5a). No appreciable changes in estimated depths and coefficients of the polynomial are found beyond the concluding iteration (Figure 5b).

The fit between the observed (solid line in black in Figure 4a) and modeled gravity anomalies at the end of the 45th iteration (solid dots in Figure 4a) is satisfactory. The estimated depths to the four density interfaces are given in Table 3 and shown graphically in Figures 4b and 4c (solid lines). The estimated coefficients of the 2nd degree polynomial to describe the fault plane are given in Table 2 and shown in Figure 4b. By and large, the modeled fault plane (simulated by a 2nd degree polynomial)

closely mimics the assumed one described by a 6th degree polynomial (Figure 4b). In this case, a maximum error of -0.022 mGal between the observed and modeled gravity anomalies is observed at the 40th km on the profile (Figure 5a). The changes in the modeled parameters (depths to density interfaces and coefficients of the 2nd degree polynomial) against the iteration number are shown in Figure 5b.

It is to be noted from Table 3 and Figure 4c that the estimated depths to the four density interfaces are marginally underestimated, with a maximum error of 5% found at the interface between vesicular and compact sediments. However, such an error between the assumed and estimated parameters is acceptable considering the presence of significant level of noise in the anomaly of the structure.

In short, the fault plane whether it is described by a 2nd degree or a 6th degree does not appreciably affect the estimated densities or depths of the formations within the hanging wall of the structure. However, the choice of a 2nd degree polynomial in the inversion would

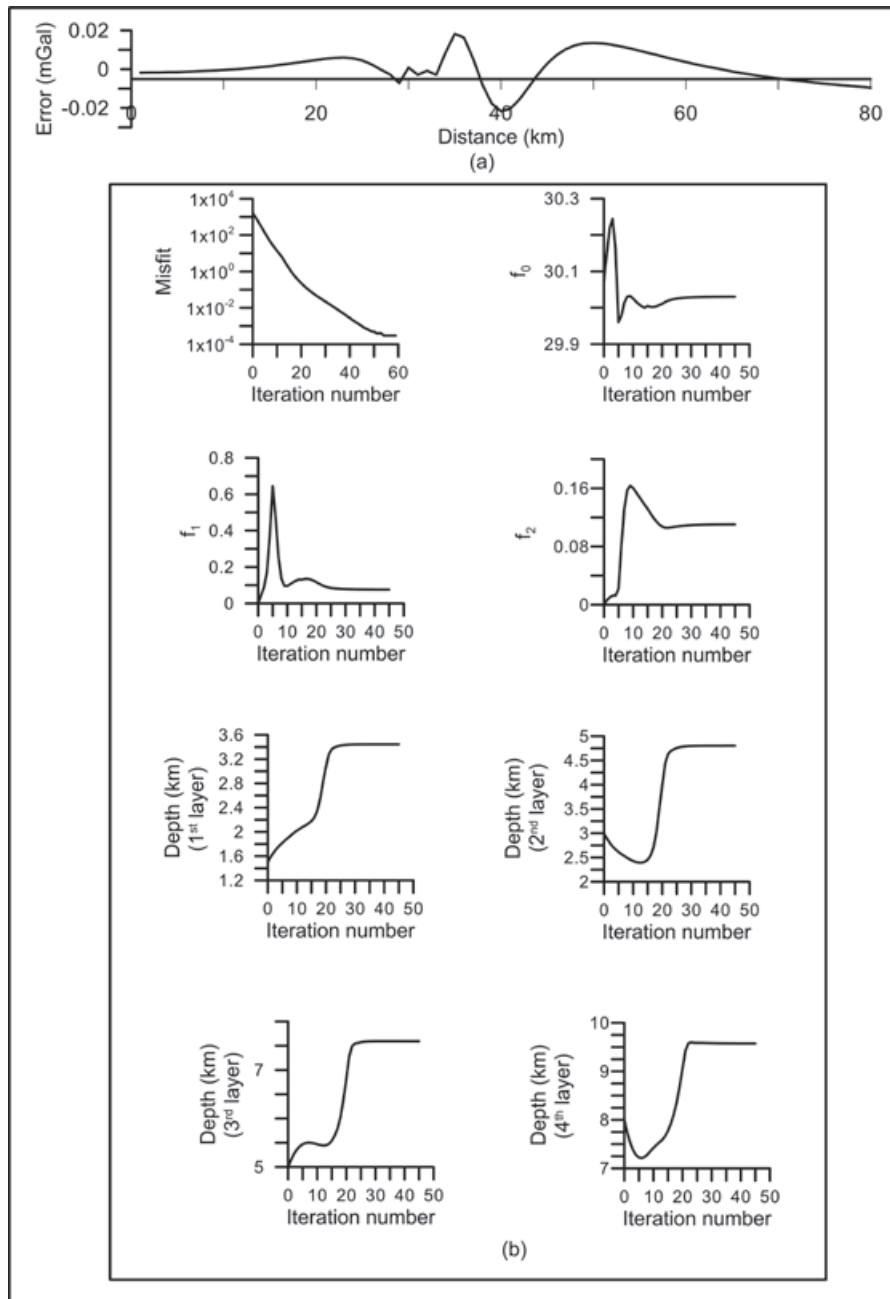


Figure 5. (a) Error analysis between the observed and modeled gravity anomalies, (b) changes in misfit, coefficients of a 2^{nd} degree polynomial, and depths of various density interfaces against the iteration number.

lead to slightly underestimate the amount of extension across normal fault when the anomalies are analyzed to estimate the depths of the density interfaces.

Field example

The proposed inversion technique is applied to analyze the gravity anomalies observed across the Aswaraopet master fault of the Chintalpudi

sub-basin in India. The interpreted results are compared with previously reported information derived from seismic refraction studies (Kaila *et al.*, 1990).

The Chintalpudi sub-basin represents the southeasterly continuation of the Pranhita-Godavari valley. Archaean gneisses (mean density 2.67 g/cm^3) form the basement for the Gondwana sequence within the sub-basin

and towards the east the basin margin is associated with the well-known Aswaraopet master fault, which is exposed at the surface and strikes NNW-SSE over a length of 20 km (Figure 6a). Kaila *et al.* (1990) have carried out Deep Seismic Sounding (DSS) investigations along a profile across the basin connecting Kallur and Polavaram (Figure 6a). The Oil and Natural Gas Corporation Ltd. (ONGC), India drilled a borehole (Figure 6a and 6c) within the basin and encountered Archaean basement at a depth of 2.935 km (Agarwal, 1995). The density contrast-depth data measured from this borehole is shown in Figure 6b (Chakravarthi, 2003). The gravity anomaly of the basin (Figure 6c) was analyzed by Chakravarthi and Sundararajan (2007) for its basement structure using a 3D inversion.

For the present study, the gravity anomalies of the basin along a profile, EE', (Figure 6a and 6c) across the Aswaraopet master fault have been analyzed using the present algorithm. This profile also forms part of the DSS profile (Figure 6a). The observed gravity anomaly along the selected profile is shown as solid

dots in Figure 7a. As in the case of synthetic example, we subject the anomaly for inversion in two ways. In either case, the fault plane is described with a 2nd degree polynomial in the inversion. The initial/approximate parameters pertaining to densities (in case of inversion performed for estimating densities and polynomial coefficients) and depths (in case of inversion performed for estimating depths and polynomial coefficients) are given in Table 4 and Table 6 and shown in Figure 7c and Figure 9c (dotted lines) respectively. Although the measured density-depth data of the basin is available, we presume different values for the parameters in the inversion to study whether the estimated parameters after the inversion mimic the measured ones or not. One can notice from Figure 7c and Figure 9c that the assumed initial parameters are significantly different from the measured quantities. The algorithm had identified the approximate location of the fault plane at 2.13 km in each case. Initially, this value was assigned to the first coefficient, f_0 , of the polynomial in either case whereas the other coefficients were set to zero.

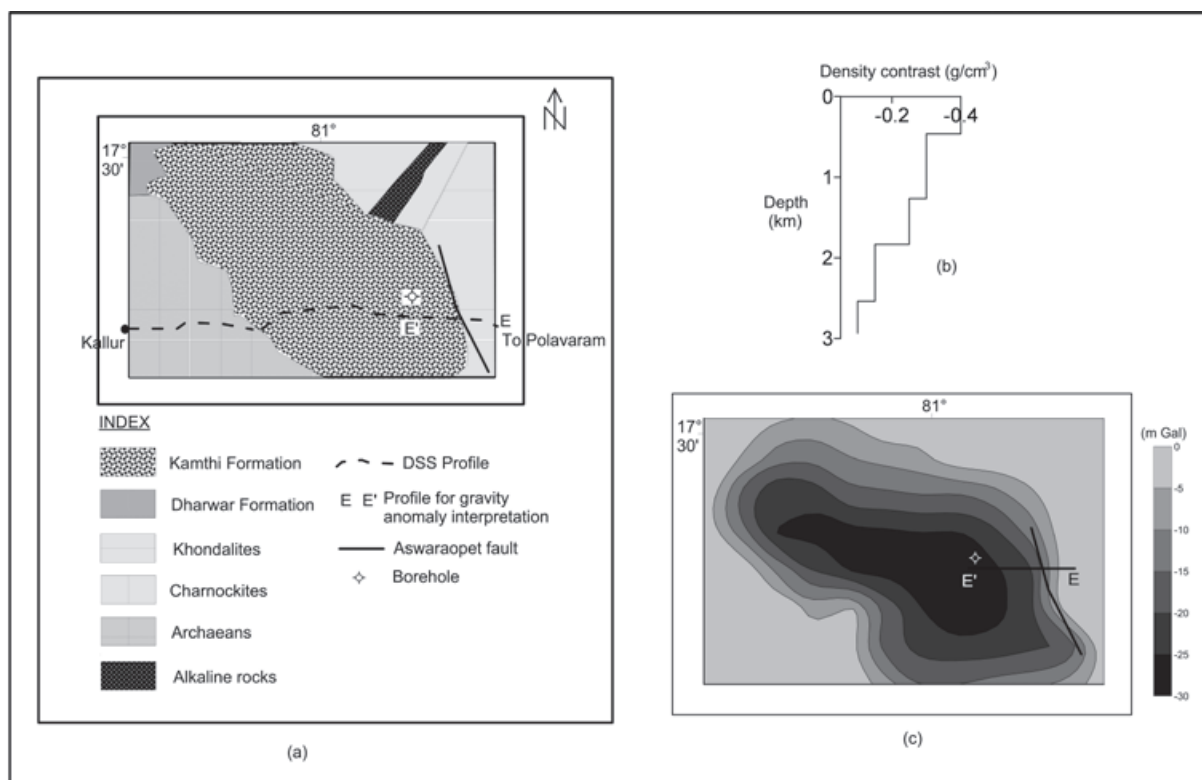


Figure 6. a) Geology of the Chintalpudi sub-basin, India (modified after Kaila *et al.* 1990), (b) measured density contrast-depth data (Chakravarthi, 2003), (c) gravity anomaly map of the Chintalpudi sub-basin, India (after Chakravarthi and Sundararajan, 2007).

Table 4. Measured and estimated densities, Chintalpudi subbasin, India.

Formation	Measured density (g/cm ³)	Initial density (g/cm ³)	Estimated density (g/cm ³)	Error (%)
1	2.27	2.0	2.279	0.396
2	2.37	2.0	2.380	0.422
3	2.42	2.0	2.410	0.410
4	2.52	2.0	2.517	0.119
5	2.57	2.0	2.562	0.311

Table 5. Estimated coefficients of the polynomial, $\zeta(z)$, Chintalpudi subbasin, India.

Coefficient	Estimated coefficients of the 2 nd degree polynomial in case of densities and fault plane inversion	Estimated coefficients of the 2 nd degree polynomial in case of depths and fault plane inversion
f_0	1.606	1.564
f_1	-0.149	0.143
f_2	0.719	0.506

Table 6. Measured and estimated depths to density interfaces, Chintalpudi subbasin, India.

Formation	Measured depth (km)	Initial depth (km)	Estimated depth (km)	Error (%)
1	0.46	0.2	0.43	6.5
2	1.265	0.9	1.10	13.0
3	1.835	1.2	1.87	1.9
4	2.54	2	2.33	8.3
5	2.935	2.5	3.01	2.5

The algorithm had performed 74 and 14 iterations in each case before terminating. The estimated parameters remained more or less unchanged beyond respective concluding iterations (Figure 8b and Figure 10b). The modeled gravity anomalies are shown in Figure 7a and Figure 9a as solid lines. The fit between the observed and modeled gravity anomalies in either case is satisfactory (Figure 7a and Figure 9a). A maximum error of 0.58 mGal between the observed and modeled gravity anomalies is observed at 6.3 km on the profile (Figure 8a) when the inversion is performed to estimate the densities and fault plane geometry. On the other hand, a maximum error of 0.64 mGal is observed at the 10th km (Figure 10a) when the anomalies are inverted for depths and fault plane geometry. The estimated density and depth parameters subsequent to respective inversions are given in Table 4 and Table 6 and shown in Figure 7c and Figure 9c respectively. The errors (%) between the estimated and

measured parameters in each case are also given in Tables 5 and 6. When the anomalies are subjected for inversion to estimate densities and the fault plane geometry, the modeled densities of the first and second formations are slightly overestimated ($\sim 0.4\%$) while others marginally underestimated (Table 4 and Figure 7c). When the inversion was performed for estimating both depths and fault plane geometry simultaneously, the modeled depths of the first, second and fourth density interfaces are modestly underestimated whereas the third and fifth density interfaces are slightly overestimated (Table 6 and Figure 9c). The changes in the estimated parameters with the iteration number in each case are shown in Fig. 8b and Figure 10b respectively.

The modeled fault plane of the structure in each case from the estimated coefficients of the 2nd degree polynomial (Table 5) is shown graphically in Figure 7b and Figure 9b. The

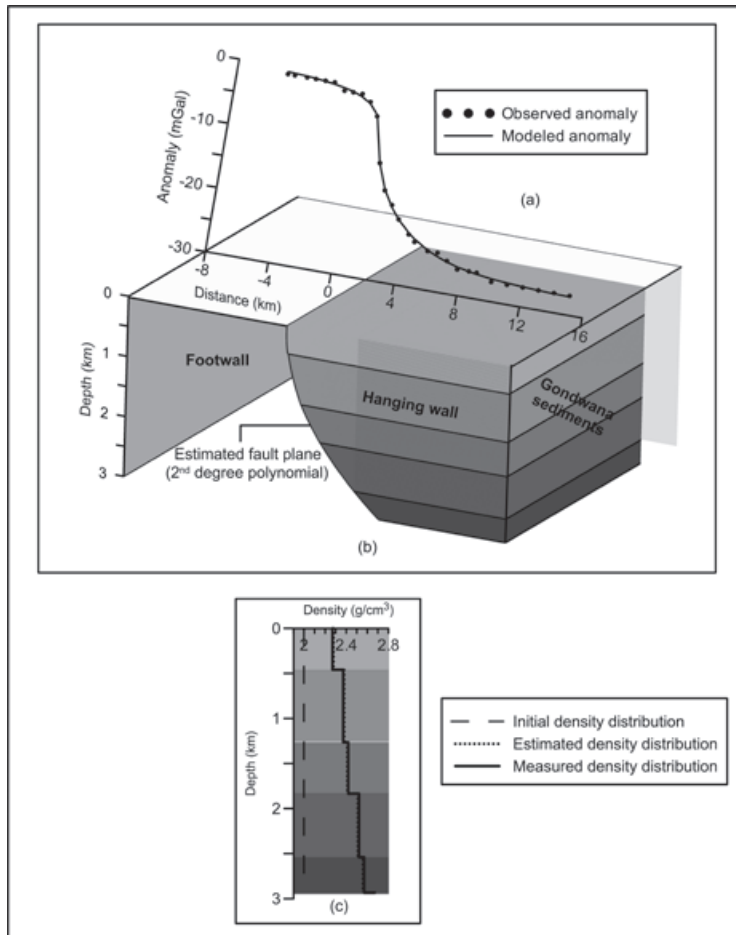


Figure 7. (a) Observed and modeled gravity anomalies, (b) inferred fault plane geometry of the Aswaraopet master fault, Chintalpudi subbasin, India, (c) assumed, initial and modeled densities. Depths of density interfaces are fixed during inversion.

Table 7. Coefficients of the 5th degree polynomial, $\zeta(z)$, used to describe the geometry of the Aswaraopet fault plane derived from DSS studies (after Kaila *et al.*, 1990).

f_0	1.852063529
f_1	-0.6020069478
f_2	-0.6020069478
f_3	0.516508814
f_4	-1.085574722
f_5	0.25061682

estimated location of the fault plane in either case from gravity modeling closely matches with the one mapped from geological studies. Furthermore, the inferred structure of the basin across the Aswaraopet fault from DSS

studies (after Kaila *et al.*, 1990) is also shown in Figure 9b for comparison. The theoretical gravity response of this structure is shown as a dashed line in Figure 9a along with the observed anomaly. In this case, a 5th degree polynomial with a set of six coefficients (Table 7) completely defines the geometry of the fault plane inferred from DSS studies. The forward modeling algorithm of Chakravarthi (2010b) is used to calculate the gravity anomalies of the structure (derived from seismic data interpretation) using the measured density-depth data (Figure 6b) of the basin. It can be seen from Figure 9a that the modeled gravity anomalies of the structure from present inversion closely mimic the observed ones, whereas the gravity response of the seismically derived structure (Kaila *et al.*, 1990) does not. In addition, the large gradient (4.5 mGal/km) in the observed anomaly between 0 and 6th km across the fault plane does not agree well with the interpretation model of Kaila *et al.* (1990), whereas it agrees reasonably well with the present gravity inversion result.

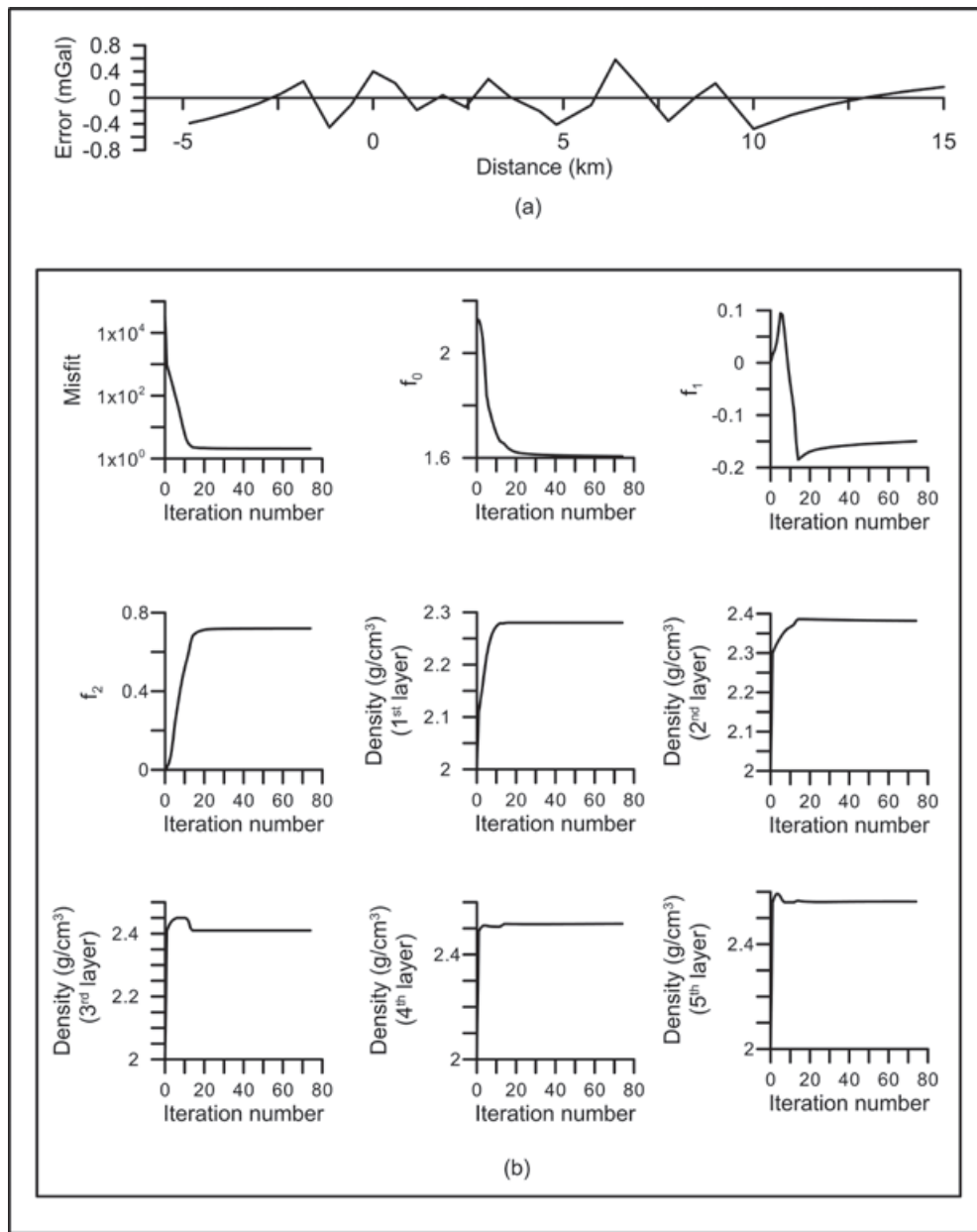


Figure 8. (a) Error analysis between the observed and modeled gravity anomalies across the Aswaraopet master fault, Chintalpudi subbasin, India, (b) Changes in misfit, coefficients of a 2nd degree polynomial, and densities of subsurface formations against the iteration number.

The structure inferred from DSS investigations (Figure 9b) shows high angle dip for the fault plane from the surface to a depth of about 0.6 km, then moderately varying dips up to 1.7 km beyond which it transforms again into a high angle normal fault. The present interpretation reveals that the fault plane (Figure 7b and Figure 9b), which dips at high

angle near the surface, shows similar dips up to a depth of 1.7 km beyond which it shows moderate dips. Further, the error (4.6%) between the measured and estimated thickness of the basin from DSS studies near the existing deep borehole is relatively more than the one estimated (2.55%) from the present inversion.

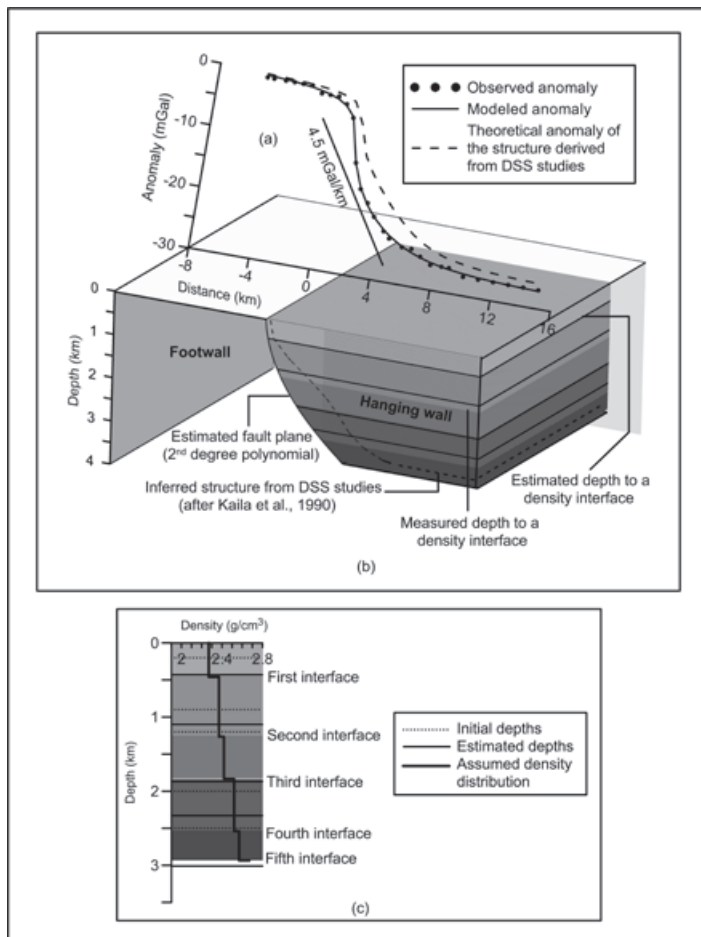


Figure 9. (a) Observed and modeled gravity anomalies, (b) inferred fault plane geometry of the Aswaraopet master fault, Chintalpudi subbasin, India. Anomalies are analyzed to estimate the depths of density interfaces.

Conclusions

A gravity inversion technique using ridge regression is presented to analyze the gravity anomalies of strike-limited listric fault sources, where the detached hanging wall of the structure consists in several geologic formations; each one possessing its own density and thickness. The fault plane is described with a polynomial function of arbitrary but specific degree. This algorithm simultaneously estimates the geometry of a fault plane and the parameters pertaining to either densities or depths of various subsurface formations from the observed gravity anomalies. The advantage of the algorithm is that it can be used to analyze the gravity anomalies of the structure even when the profile along which the interpretation is intended fails to bisect the fault plane.

The algorithm is applied to both synthetic and real field gravity anomalies. In case of synthetic example; significant level of pseudorandom noise was added to the gravity anomalies produced by a structure, whose

fault plane was described with a 6th degree polynomial. To study the effect of the choice of the degree polynomial in the interpretation, the noisy anomalies were inverted presuming a 2nd degree polynomial for the fault plane. The noisy anomalies were then analyzed to estimate i) the densities and fault plane geometry, keeping the depths of density interfaces unchanged, and ii) depths and fault plane geometry, keeping densities intact. In either case, the estimated parameters pertaining either to densities or depths closely mimic the assumed parameters. However, the choice of the lower order polynomial (such as a 2nd degree) would lead to marginally underestimate the amount extension across the normal fault, when inversion is performed to estimate the fault plane geometry and depths of density interfaces.

The observed gravity anomalies across the Aswaraopet master fault from the eastern margin of the Chintalpudi subbasin in India are analyzed by the proposed technique and found that the estimated parameters (densities

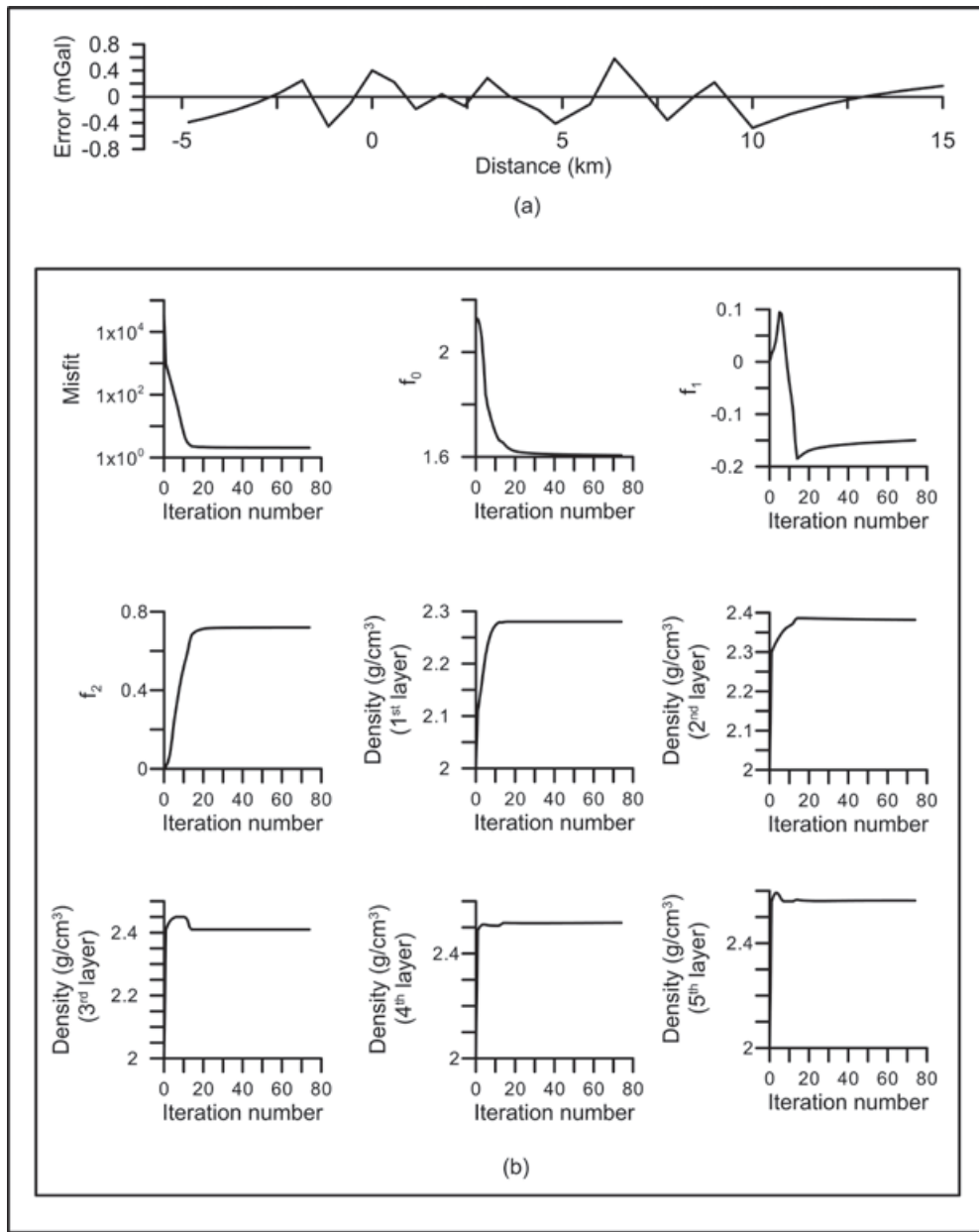


Figure 10. (a) Error analysis between the observed and modeled gravity anomalies across the Aswaraopet master fault, Chintalpudi subbasin, India, (b) changes in misfit, coefficients of a 2nd degree polynomial, and depths to various density interfaces against the iteration number.

and thicknesses of subsurface formations within the hanging wall) from independent gravity inversion reasonably coincide with the measured ones. On the other hand, the calculated gravity response of the structure derived from seismic data interpretation (Kaila *et al.* 1990) using the measured density-depth data significantly deviates from the observed anomaly. Further, the large gradient in the observed gravity anomaly over the fault plane is better explained by the gravity inversion

model rather than the one reported from seismic data interpretation (Kaila *et al.*, 1990).

However, the proposed inversion technique presumes that the detached hanging wall of listric fault morphology consists in several geologic formations with each one bounded on top and bottom by flat surfaces, which in reality may or not be valid. Therefore, the inversion technique is more effective when the assumptions are relatively valid.

Acknowledgements

The authors profusely thank the anonymous reviewers for their critical reviews and many useful suggestions to improve the manuscript as presented.

References

Agarwal B.P., 1995, Hydrocarbon prospects of the Pranhita-Godavari graben, India. *Proceedings of Petrotech*. 95, 115-121.

Abdelrahman E.M., Bayoumi A.I., El-Araby H.M., 1989, Dip angle determination of fault planes from gravity data. *Pure and Applied Geophysics*, 130, 4, 735-742.

Abdelrahman E.M., El-Araby H.M., El-Araby T.M., Abo-Ezz E.R., 2003, A least-squares derivatives analysis of gravity anomalies due to faulted thin slabs. *Geophysics*, 68, 535-543.

Adriasyah A., McMechan A.G., 2002, Analysis and interpretation of seismic data from thin reservoirs: Northwest Java basin, Indonesia. *Geophysics*, 67, 14-26.

Brady R., Wernicke B., Fryxell J., 2000, Kinematic evolution of a large-offset continental normal fault system; South Virgin Mountains, Nevada. *Geological Society of America Bulletin* 112, 1375-1397.

Chakravarthi V., Ramamma B., (2013), Gravity anomaly modeling of multiple geological sources having different strike lengths and arbitrary density contrast variations. *Near Surface Geophysics*, 11, 4, 363-370.

Chakravarthi V., 2011, Automatic gravity optimization of 2.5D strike listric fault sources with analytically defined fault planes and depth-dependent density. *Geophysics*, 76, I21-I31.

Chakravarthi V., 2010, Gravity anomalies of strike limited listric fault sources with analytically defined fault planes and arbitrary density contrast variations with depth. *Near Surface Geophysics*, 8, 279-286.

Chakravarthi V., 2003, Digitally implemented method for automatic optimization of gravity fields obtained from three-dimensional density interfaces using depth dependent density. *United States Patent*, 6,615,139.

Chakravarthi V., Sundararajan N., 2007, 3D gravity inversion of basement relief - A depth dependent density approach. *Geophysics*, 72, I 23- I 32.

Chakravarthi V., Sundararajan N., 2006, Gravity anomalies of multiple prismatic structures with varying density - A Marquardt inversion. *Pure and Applied Geophysics*, 163, 229-242.

Chakravarthi V., Sundararajan N., 2004, Ridge regression algorithm for gravity inversion of fault structures with variable density. *Geophysics*, 69, 1394-1404.

Chakravarthi V., Singh S.B., Ashok Babu G., 2001, INVER2DBASE - A program to compute basement depths of density interfaces above which the density contrast varies with depth. *Computers & Geosciences*, 27, 1127-1133.

Essa K.S., 2013, Gravity interpretation of dipping faults using the variance analysis method. *Journal Geophysics and Engineering*, 10, 015003.

Goussev S., Charters R., Peirce J., 2006, Mackenzie Delta: A case of one residual gravity anomaly and 16 dry exploration wells. 2006 CSPG/CSEG/CWLS Joint Conference, 15-18 May, Calgary, Canada, Expanded Abstracts, 435-439.

Gómez-Ortiz D., Tejero-López R., Babín-Vich R., Rivas-Ponce A., 2005, Crustal density structure in the Spanish Central System derived from gravity data analysis (Central Spain). *Tectonophysics*, 403, 131-149.

Kaila K. L., Murthy P. R. K., Rao V. K., Venkateswarlu N., 1990, Deep seismic sounding in the Godavari Graben and Godavari (Coastal) Basin, India. *Tectonophysics*, 173, 307-317.

Marquardt D. W., 1970, Generalized inverses, ridge regression, biased linear estimation, and nonlinear estimation. *Technometrics*, 12, 591-612.

Martín-Atienza B., García-Abdeslem J., 1999, 2-D gravity modeling with analytically defined geometry and quadratic polynomial density functions. *Geophysics*, 64, 1730-1734.

Maxant J., 1980, Variation of density with rock type, depth, and formation in the Western

Canada basin from density logs. *Geophysics*, 45, 1061-1076.

McKenzie D., 1978, Some remarks on the development of sedimentary basins. *Earth and Planetary Science Letters*, 40, 25-32.

McKenzie D., Jackson J., 2012, Tsunami earthquake generation by the release of gravitational potential energy. *Earth and Planetary Science Letters*, 345-348, 1-8.

Moral C. R., Gómez Ortiz D., Tejero R., 2000, Spectral analysis and gravity modelling of the Almazán basin (Central Spain). *Journal of the Geological Society of Spain*, 13, 131-142.

Murthy I.V.R., Krishnamacharyulu S.K.G., 1990, Automatic inversion of gravity anomalies of faults. *Computers & Geosciences*, 4, 539-548.

Nagihara S., Hall S.A., 2001, Three-dimensional gravity inversion using simulated annealing: constraints on the diapiric roots of allochthonous salt structures. *Geophysics*, 66, 1438-1449.

Peirce J.W., Lipkov L., 1988, Structural interpretation of the Rukwa rift, Tanzania. *Geophysics*, 53, 824-836.

Rao D.B., 1985, Analysis of gravity anomalies over an inclined fault with quadratic density function. *Pure and Applied Geophysics*, 123, 250-260.

Rao M. M. M., Murthy T.V.R., Murthy K.S.R., Vasudeva R.Y., 2003, Application of natural generalized inverse technique in reconstruction of gravity anomalies due to a fault. *Indian Journal of Pure and Applied Mathematics*, 34, 31-47.

Rybakov M., Goldshmidt V., Fleischer L., Ben-Gai Y., 2000, 3-D gravity and magnetic interpretation for the Haifa Bay area (Israel). *Journal of Applied Geophysics*, 44, 353-367.

Stavrev P., Reid A., 2010, Euler deconvolution of gravity anomalies from thick contact/fault structures with extended negative structural index. *Geophysics*, 75, I51-I58.

Sundararajan N., Ramabrahmam G., 1998, Spectral analysis of gravity anomalies caused by slab-like structures: A Hartley transform technique. *Journal of Applied Geophysics*, 39, 53-61.

Thanassoulas C., Tselentis G.A., Dimitriadis K., 1987, Gravity inversion of a fault by Marquardt's method. *Computers & Geosciences*, 13, 399-404.

Toushmalani R., 2013, Gravity inversion of a fault by particle swarm optimization. *SpringerPlus*, 2:315.